

Assaf Zemel · Avinoam Ben-Shaul · Sylvio May

Perturbation of a lipid membrane by amphipathic peptides and its role in pore formation

Received: 2 August 2004 / Accepted: 8 October 2004 / Published online: 24 December 2004
© EBSA 2004

Abstract We study the structural and energetic consequences of (α -helical) amphipathic peptide adsorption onto a lipid membrane and the subsequent formation of a transmembrane peptide pore. Initially, each peptide binds to the membrane surface, with the hydrophobic face of its cylinder-like body inserted into the hydrocarbon core. Pore formation results from subsequent peptide crowding, oligomerization, and eventually reorientation along the membrane normal. We have theoretically analyzed three peptide–membrane association states: interfacially-adsorbed monomeric and dimeric peptides, and the multi-peptide transmembrane pore state. Our molecular-level model for the lipid bilayer is based on a combination of detailed chain packing theory and a phenomenological description of the headgroup region. We show that the membrane perturbation free energy depends critically on peptide orientation: in the transmembrane pore state the lipid perturbation energy, per peptide, is smaller than in the adsorbed state. This suggests that the gain in conformational freedom of the lipid chains is a central driving force for pore formation. We also find a weak, lipid-mediated, gain in membrane perturbation free energy upon dimerization of interfacially-adsorbed peptides. Although the results pertain mainly to weakly-charged peptides, they reveal general properties of the interaction of amphipathic peptides with lipid membranes.

Introduction

Many naturally occurring α -helical, amphipathic peptides, such as melittin, magainins, dermaseptins, pardaxins, or alamethicin, are able to perforate lipid bilayers by forming membrane pores. The level of activity and selectivity possessed by these membrane-active peptides is intimately related to the physical properties of the target membrane. Most notably, no specific binding site is required; membrane adsorption is typically driven by hydrophobic interaction with the hydrocarbon chain region of the membrane and, when the peptides are charged, by electrostatic attraction to oppositely-charged lipids. Individual membrane-associated peptides orient horizontally at the hydrocarbon–water interface of the target monolayer, embedding their hydrophobic faces into the hydrocarbon core of the membrane. Above a sufficiently high concentration of adsorbed peptides, pore formation sets in by a cooperative process that involves the self-assembly of several (typically 3–10) peptides. This is accompanied by an orientational change in the pore-forming peptides, upon which the long axis of the amphipathic α -helix reorients normal to the bilayer plane. Rearrangement into a transmembrane-inserted ring-like aggregate with the hydrophobic peptide residues pointing towards the lipids chains results in a water-filled pore with subsequent loss of the membrane's permeability barrier.

Oren and Shai (Oren and Shai 1998) have classified amphipathic peptides into two distinct groups according to the mechanism by which they disintegrate the membrane. Underlying the difference between the two groups of peptides is their tendency to self-associate in the target membrane. One group consists of weakly-charged peptides (net charge ≈ 1), like alamethicin and pardaxin, for which binding essays and leakage measurements (of dye markers from lipid vesicles) indicate that self-association occurs even at very low peptide concentrations, where the bound peptide/lipid ratio is less than 1/1000 (Rapaport et al. 1996; Schwarz et al. 1986; Rapaport

A. Zemel · A. Ben-Shaul (✉)
Department of Physical Chemistry
and the Fritz Haber Research Center,
The Hebrew University, Jerusalem, 91904, Israel
E-mail: abs@fh.huji.ac.il
Tel.: +972-2-6585271
Fax: +972-2-6513742

S. May
Junior Research Group “Lipid Membranes”,
Friedrich-Schiller-Universität Jena, Neugasse 25,
Jena, 07743, Germany

and Shai 1991, 1992). It has been suggested that self-association occurs prior to pore formation, presumably on the membrane surface. Notably, only a small fraction of the interfacially-bound peptides change their orientation into a transmembrane configuration. The horizontal orientation maintained by most membrane-bound peptides is evidenced by oriented circular dichroism measurements; the majority of alamethicin molecules adopt the transmembrane orientation only at peptide/lipid ratios larger than 1/100 (Huang and Wu 1991). The propensity of these peptides to aggregate on the membrane surface, even at low peptide/lipid ratios, suggests that an attractive, presumably lipid-mediated, force operates between them. Moreover, it is believed that weakly-charged peptides form rather small and tightly packed pores, often described as barrel-stave pores. Theoretical modeling (Zemel et al. 2003) indeed suggests that electrostatic repulsion between the charged peptides within the pore is not strong enough to widen the pore beyond the steric size of the “barrel-staves”.

The other group of peptides comprises highly-charged (usually cationic) peptides (net charge ≥ 4) such as melittin, magainin, and cecropin. These peptides do not self-associate at low peptide concentrations; rather, they are uniformly spread across the membrane surface, forming a “carpet” even at high peptide concentrations (Oren and Shai 1998). The cooperative assembly of pores occurs only when the concentration of adsorbed peptides exceeds a certain limiting value, corresponding to a peptide/lipid ratio larger than 1/100 (Ludtke et al. 1994; Yang et al. 2001; Dempsey et al. 2003; Bechinger 1999). The resulting pore structure has been characterized based on both experimental observations (Matsuzaki et al. 1998; Ludtke et al. 1996; Yang et al. 2000, 2001) and theoretical calculations (Lin and Baumgaertner et al. 2000; Zemel et al. 2003). The so-called “toroidal pores” comprise a bundle of transmembrane peptides, interspaced by 1–2 nm segments of a semitoroidal lipid rim. The formation of an intervening lipid rim allows the highly-charged peptides to separate while partially shielding lipid tails from contact with water.

Pore formation involves peptide oligomerization and thus requires an energetic incentive to overcome the entropic penalty. For high peptide/lipid concentrations the lateral pressure exerted by the interfacially adsorbed “gas” of peptides provides a strong driving force towards pore formation (Zuckermann and Heimburg 2001). An alternative and complementary explanation has been given by Huang and coworkers (Huang et al. 2004; He et al. 1996; Chen et al. 1997). This model attributes the cooperative process of pore formation to the relief of internal membrane stress, stored upon the adsorption of peptides in its interface. Membrane thinning was suggested to be the main indication of lipid perturbation. X-ray measurements of membrane thickness reveal a linear decrease in membrane thickness upon increasing the peptide/lipid ratio (He et al. 1996; Chen et al. 1997). NMR measurements of lipid chain bond orientational order parameter profiles provide

another indication of membrane thinning. Typically, these measurements show a net reduction in chain ordering (Koenig et al. 1999). Above a critical peptide/lipid ratio, the peptides undergo a collective orientational change into the peptide pore state, resembling a membrane phase transition. The existence of water-filled pores above the critical concentration has been monitored by in-plane neutron scattering experiments (Ludtke et al. 1995, 1996), while in turn, X-ray measurements show that the thickness of the membrane remains unchanged (He et al. 1996; Chen et al. 1997; Huang et al. 2004). The theoretical model of Huang et al. (2004) correctly predicts the concentration dependence of peptide orientation and membrane thickness over a wide range of concentrations, including the behavior near the transition point.

For low peptide concentrations, pore formation must be driven by a direct or local membrane-mediated peptide–peptide interaction. Indeed, the kinetics of pore formation depend upon the existence of intermediate aggregates, such as transient self-associated dimers and trimers. Recent kinetic (Takei et al. 1999) and equilibrium studies (Dempsey et al. 2003; Hristova et al. 2001) using cross-linked disulfide-dimerized melittin and magainin analogs, support the idea that an interfacially adsorbed, self-associated dimer acts as a precursor or a meta-stable intermediate in the pore-formation mechanism. The use of a dimerized melittin analog in a kinetic experiment to measure pore formation rates, has been shown to reduce the molecularity of the process, indicating that peptide dimerization is a rate limiting step (Takei et al. 1999). The dimerized magainin analog shows enhanced membrane permeabilization activity compared with the corresponding monomer. Pore formation by the dimerized peptide occurs well below the monomers’ threshold concentration. Significant leakage of dye markers from lipid vesicles have been measured at peptide-to-lipid ratios as low as 1/5000. The dependence on peptide concentration was found to be much weaker, namely less cooperative, for the dimerized peptide (Dempsey et al. 2003). It was suggested that membrane perturbation resulting from the formation of the peptide dimer is the essential event that triggers the change in peptide orientation and the formation of a pore (Hristova et al. 2001).

In the present work, we analyze the energetics of pore formation, focusing on the role of the lipid bilayer in peptide assembly and reorientation. To this end, a molecular-level mean-field theory of chain packing in lipid membranes is used to calculate free energies of various bilayer-peptide configurations. To capture the universal features of pore formation we refrain from including specific peptide–lipid and peptide–peptide interactions. Thus α -helical amphipathic peptides are simply modeled as bulky (cylinder-like) inclusions that perturb the lipid chain packing in the hydrocarbon core of the target membrane. The nature of the perturbation depends on the orientation of the peptides. We will show that interfacially-adsorbed peptides which adopt a

horizontal orientation with respect to the membrane plane perturb the lipid bilayer significantly more severely than transmembrane peptides that form barrel-stave pores. Based on this observation, we suggest that the orientational dependence of the peptide-induced membrane perturbation provides a generic and unspecific driving force for pore formation. Our model is applicable for weakly-charged peptides in the limit of small peptide concentrations on the membrane. The propensity of peptides to self-assemble into barrel-stave pores in such a scenario is yet to be explained satisfactorily.

We also use our model to characterize the first step in the self-association of peptides on the membrane, namely peptide–peptide dimerization. In line with our previous work (Zemel et al. 2004), we predict that a weak, lipid-mediated, attractive force acts between two parallel, interfacially-adsorbed peptides. We estimate the membrane contribution to the dimerization free energy to be on the order of $k_B T$ (k_B is the Boltzmann constant and T is the absolute temperature). We argue that this is slightly larger than the opposing electrostatic repulsion for weakly-charged peptides, but too small to drive the association of highly-charged peptides. Hence, our analysis suggests that pore formation is primarily regulated on the level of the self-association process where highly and weakly-charged peptides reveal different kinetic behaviors.

Theory

We apply our theoretical model to study the structural and energetic consequences of lipid chain packing in three different peptide–membrane association states that are depicted in Fig. 1: interfacially adsorbed monomeric (well separated) peptides (a), interfacially adsorbed peptide dimers (b), and aggregated peptides forming a barrel-stave pore (c). In all cases, the membrane consists of two (possibly perturbed) monolayers, an inner monolayer and an outer one. We shall use the symbol \mathcal{A} to denote the (shape and area of the) interface between the apolar hydrocarbon core and the lipid headgroup region. The surface area of \mathcal{A} is $A = N\bar{a}_i$ where N is the number of lipid chains in the membrane and \bar{a}_i is the average cross-sectional area per chain, measured at \mathcal{A} . The lipid volume enclosed by \mathcal{A} , namely the hydrocarbon core, will be denoted by \mathcal{V} ; and the embedded part of the peptide by \mathcal{V}_p .

Free energy per molecule

Peptide adsorption or insertion modifies the packing characteristics of the lipid molecules as compared to those of the unperturbed (peptide-free) membrane. The total membrane perturbation free energy, F , is then a sum of local contributions, $f(\mathbf{r}) - f_0$, where $f(\mathbf{r})$ is the local free energy per molecule at \mathbf{r} (\mathbf{r} denoting the position of its headgroup at \mathcal{A}) and f_0 is the corresponding free

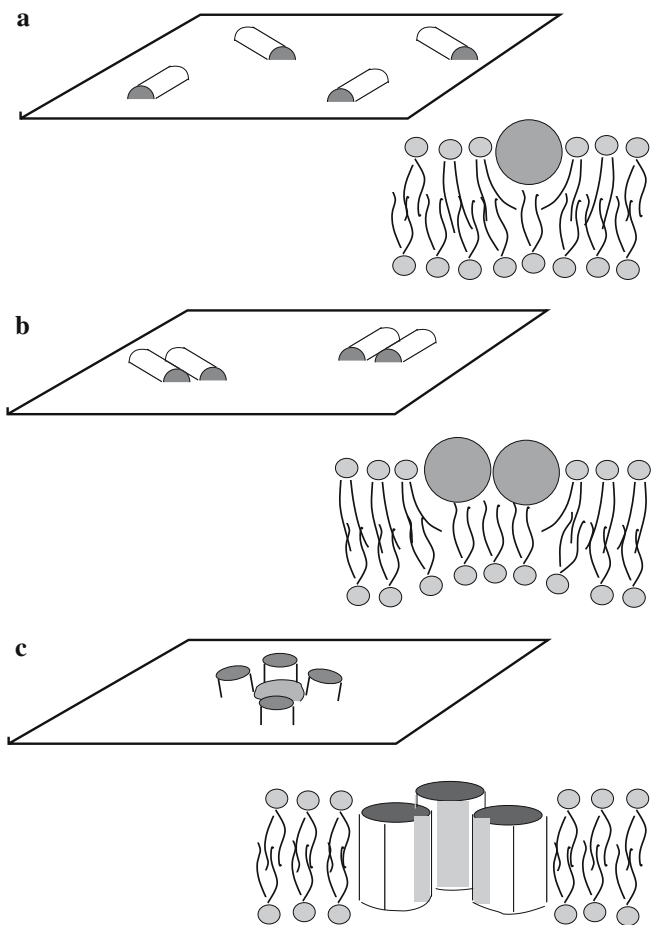


Fig. 1 Schematic illustration of the three membrane-peptide association states analyzed in the present work. The peptides are represented as interfacially adsorbed monomeric (a) and self-associated dimeric (b) cylinders, or as a barrel-stave pore (c) with the peptides oriented in the transmembrane direction. In the membrane cross-sections we have schematically depicted some lipids to illustrate that peptide adsorption, self-association, and subsequent reorientation involves changes in lipid packing order

energy in the peptide-free membrane. Our model for calculating f consists of a detailed, molecular level, mean-field theory for the conformational statistics of the lipid tails, combined with phenomenological descriptions of both lipid headgroup interactions and of the interfacial energy between the apolar hydrocarbon core and the polar headgroup region. Assuming additivity of these three contributions, we write for the free energy per lipid molecule

$$f = f_h + f_i + f_c \quad (1)$$

The head group and interfacial contributions, $f_h = B/a_h$ and $f_i = \gamma a_i$, respectively, are modeled in a similar way to the opposing forces model (Israelachvili 1992); B measures the strength of headgroup repulsion and γ is the interfacial tension between the hydrocarbon chains and the polar environment (we shall use $\gamma = 0.12 k_B T/\text{\AA}^2 \approx 50$ dynes/cm in our numerical calculations (Israelachvili 1992)). The magnitudes of the cross-sectional area per

molecule, a_h and a_i , measured at the headgroup and hydrocarbon–water reference surfaces, depend on the molecular packing properties of the lipid molecule. Explicitly, a_i is the local cross-sectional area per lipid, measured at \mathcal{A} , and $a_h = a_i [1 + (c_1 + c_2)l + c_1 c_2 l^2]$ is the corresponding cross-sectional area at the headgroup region, measured in a parallel surface at distance l away from \mathcal{A} (see Fig. 2). Here c_1 and c_2 are the local principal curvatures of \mathcal{A} (by convention we assign positive curvature to an outwardly bent surface). Although approximate, our models for f_h and f_i are known to provide a useful representation of the energetics and preferred aggregation behavior of lipid assemblies (Israelachvili 1992). For example, they can be used to predict common elastic properties of lipid monolayers or bilayers, like the bending stiffness or spontaneous curvature (Helfrich 1973) as a function of molecular interaction parameters (May and Ben-Shaul 1999; May 2000).

The presence of membrane-inserted peptides not only affects the conformational properties of the neighboring lipid tails but may also affect the shape of the host membrane, as reflected by the geometry of the interfacial surface \mathcal{A} . Modeling of these subtle effects requires an accurate model for the lipid tail's free energy f_c . In the following, we outline the basic features of the molecular-level chain packing theory that we employ for f_c in this work (for other applications see Ben-Shaul and Gelbart 1994).

Consider a lipid tail that originates at position \mathbf{r} on \mathcal{A} . (Because all lipid chains—no matter whether they originate from the same or from different headgroups—are

treated on the same mean-field level, it is convenient to assume that each lipid involves only one hydrocarbon chain. Application of our results to double-tailed lipids is then straightforward.) Any conformation α of the chain is adopted with (an as yet unspecified) probability $P(\alpha|\mathbf{r})$; this probability vanishes for all *non-accessible* chain conformations, those that penetrate either into the aqueous environment or cross the peptide envelope. Thus, all chains with *accessible* conformations are contained entirely within \mathcal{V} . Note that $P(\alpha|\mathbf{r})$ is a conditional probability; hence the normalization $\sum_{\alpha} P(\alpha|\mathbf{r}) = 1$ for any given \mathbf{r} . Denoting the corresponding internal (trans/gauche) energy of the chain by $\epsilon(\alpha)$, we write for the conformational free energy $f_c = f_c(\mathbf{r})$ of the chain

$$f_c = \sum_{\alpha} P(\alpha|\mathbf{r}) [\epsilon(\alpha) + k_B T \ln P(\alpha|\mathbf{r})] \quad (2)$$

where the sum extends over all accessible chain conformations.

Total free energy

The total free energy of the lipid-peptide membrane is obtained by summing up the free energies of all individual lipid chains. Using $\sigma(\mathbf{r}) = 1/a_i(\mathbf{r})$ to denote the local area density of chains, attached at position r to the interfacial surface \mathcal{A} (of either the external or internal monolayer) we have

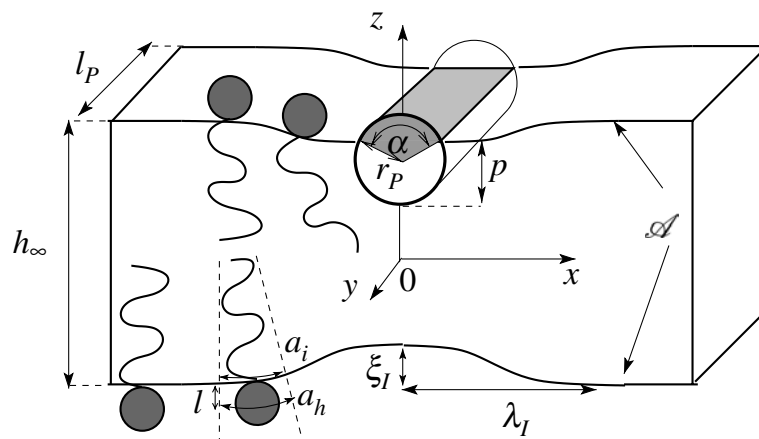
$$\int_{\mathcal{A}} d^2 r \sigma(\mathbf{r}) = N \quad (3)$$

where N is the overall number of lipid chains in the bilayer.

If σ and f are known at all positions \mathbf{r} along the surface \mathcal{A} of the two monolayers, we can calculate the free energy of the peptide-containing membrane through

$$F = \int_{\mathcal{A}} d^2 r \sigma(\mathbf{r}) \left[f(\mathbf{r}) + k_B T \ln \frac{\sigma(\mathbf{r})}{\bar{\sigma}} \right] \quad (4)$$

Fig. 2 Schematic illustration of a lipid bilayer, containing one, partially inserted, cylindrical amphipathic peptide with a radius r_P and a polar angle α which defines the insertion depth p of the peptide. The shape modulation of the membrane is modeled by two sinusoidal functions; see Eqs. 10 and 11. The xy -plane coincides with the membrane midplane far from the peptide, where the thickness of the membrane's hydrocarbon core relaxes to h_{∞} . The y -axis is parallel to the long axis of the cylinder-like peptide. For one lipid we plot the local interfacial cross-sectional area, a_i (measured on \mathcal{A}) and the local headgroup area, a_h (measured at distance l away from \mathcal{A})



The second term in Eq. 4 accounts for the demixing free energy of the lipid head groups, associated with deviations of the local headgroup density, $\sigma(\mathbf{r})$, from the uniform distribution $\bar{\sigma} = 1/\bar{a}_i$.

Constraint of uniform chain packing

As in previous work, we minimize F subject to a single packing constraint expressing the condition of a uniform, liquid-like, density of the hydrocarbon core of the membrane. To formulate the constraint, consider a chain in conformation α attached at position r to the interface \mathcal{A} and let $\phi(\alpha, \mathbf{r}', \mathbf{r})$ denote the number of segments of this chain residing in the small volume element $d^3\mathbf{r}'$ at position \mathbf{r}' within the hydrocarbon core \mathcal{V} . (Of course, if the distance $|\mathbf{r}-\mathbf{r}'|$ exceeds the length of a fully stretched (all-trans) chain then $\phi=0$.) Averaging over all conformations of all lipid chains yields the average number density of chain segments at any given location \mathbf{r}' within the hydrocarbon core

$$\langle \phi(\mathbf{r}') \rangle = \frac{1}{N} \int_{\mathcal{A}} d^2r \sigma(\mathbf{r}) \sum_{\alpha} P(\alpha|\mathbf{r}) \phi(\alpha, \mathbf{r}', \mathbf{r}) = \bar{\phi} \quad (5)$$

The second equality in Eq. 5 represents the constraint of uniform chain segment density at any given \mathbf{r}' . In the liquid-like membrane $\bar{\phi} = 1/Nv$ where v is the volume per chain segment in the hydrophobic core. In the present work, we consider membranes composed of C-12 chains (lauric acids), $\text{COOH}-(\text{CH}_2)_{10}-\text{CH}_3$. Each methylene group, occupying a volume $v \approx 27 \text{ \AA}^3$, is counted as one ‘‘chain segment’’, whereas the terminal methyl group is approximately twice as large and will be counted as two chain segments. The chain volume is thus $v \approx 13 \times v = 351 \text{ \AA}^3$.

Free energy minimization

The free energy F must be minimal with respect to both the chain probabilities, $P(\alpha|\mathbf{r})$, and the area density, $\sigma(\mathbf{r})$, subject to the constraint of uniform chain packing; see Eq. 5. The former minimization results in

$$P(\alpha|\mathbf{r}) = \frac{\chi(\alpha, \mathbf{r})}{q(\mathbf{r})} \quad (6)$$

where $\chi(\alpha, \mathbf{r})$ is the Boltzmann weighting factor

$$\chi(\alpha, \mathbf{r}) = \exp \left[-\frac{1}{k_B T} \left(\varepsilon(r) + \int_{\mathcal{V}} d^3r' \lambda(\mathbf{r}') \phi(\alpha, \mathbf{r}', \mathbf{r}) \right) \right] \quad (7)$$

The local partition function $q(\mathbf{r}) = \sum_{\alpha} \chi(\alpha, \mathbf{r})$ ensures the normalization of $P(\alpha|\mathbf{r})$. The function $\lambda(\mathbf{r})$ represents the set of Lagrangian multipliers that must be determined so as to satisfy the constraint of uniform chain

packing density everywhere within \mathcal{V} (see below).

Minimization with respect to σ yields

$$\frac{\sigma(\mathbf{r})}{\bar{\sigma}} = \frac{q(\mathbf{r})}{q} \exp \left(-\frac{2\tilde{B}\sigma(\mathbf{r})}{k_B T} \right) \quad (8)$$

where $\tilde{B} = B/[1 + (c_1 + c_2)l + c_1c_2l^2]$ and where again the partition function

$$q = \frac{\bar{\sigma}}{N} \int_{\mathcal{A}} d^2r q(\mathbf{r}) \exp \left(-\frac{2\tilde{B}\sigma(\mathbf{r})}{k_B T} \right) \quad (9)$$

ensures the normalization condition Eq. 3. Equation 9 represents a nonlinear equation for the chain density σ which must be solved numerically for each interfacial position \mathbf{r} on \mathcal{A} . At the same time, the Lagrangian multipliers, $\lambda(\mathbf{r})$, are calculated at each position r within the hydrocarbon core \mathcal{V} by solving the self-consistency relation that follows by inserting Eq. 6 into the uniform density constraint Eq. 5; see also (Zemel et al. 2004).

At this point, we note that the minimization with respect to σ not only optimizes the lateral distribution of the lipid chains within a given monolayer, but also accounts for optimal exchange (flip-flop) of the lipids between the two monolayers of a bilayer. Suppressing flip-flop implies an additional constraint in the minimization of F ; however, this case is not considered here.

Specification of membrane geometry

The formalism presented above can be applied to a membrane of any given interfacial shape, \mathcal{A} , in the presence or the absence of membrane-inserted peptides. However, optimization of the membrane shape for a given peptide arrangement is a difficult task because the free energy of the lipid chains is non-local and thus does not allow us to perform a functional minimization. Moreover, the numerical calculation of F for a complex membrane shape \mathcal{A} is computationally very costly. Consequently, we introduce a number of geometrical simplifications which nevertheless preserve the principal mechanism of peptide-induced pore formation.

Isolated, interfacially-adsorbed peptides

Consider first the non-aggregated state where individual peptides are interfacially adsorbed onto the outer monolayer of a flat membrane; see Fig. 1a. (We note that the flatness of the membrane is an assumption, appropriate, for example, for bilayers in the lamellar L_{α} phase, or for a membrane on a flat solid support. A more general—but computationally much more involved—approach would allow the peptides to induce an overall bending of the membrane; however, the corresponding energy changes are not expected to affect the conclusions of the present work.) Neglecting atomic details, the peptides are modeled as cylinders of length l_p

and radius r_P , whose mantle subtends the “hydrophilic” angle α and a complementary “hydrophobic” angle $2\pi-\alpha$. In the present study, we shall focus on a representative case where $\alpha=\pi$. The hydrophobic part of each peptide is modeled as being inserted into the hydrocarbon core of the outer monolayer, with the peptide’s long axis being parallel to the bilayer midplane. Owing to the elongated shape of the peptides, the packing properties of the lipids around each individual peptide will predominantly vary in the direction perpendicular to rather than along the peptide’s long axis. Variations along the latter axis arise mainly from perturbations of chain packing around the peptide ends. We shall neglect these end effects and treat the packing of the lipid molecules as invariant along the peptide’s long axis.

Let the z -axis of a Cartesian coordinate system point normal to the (flat) bilayer midplane, and let the long axis of the peptide be parallel to the y -direction. The interfacial shape of the membrane, \mathcal{A} , will then only vary along the x -direction; see Fig. 2. Hence, we can characterize the shape of the outer and inner monolayers by the two functions $z_E(x)$ and $z_I(x)$, respectively. We assume that these functions can be expressed parametrically in the form

$$z_E(x) = \frac{\xi_E}{2} \left(\cos \frac{\pi(x-r_P)}{\lambda_E} + 1 \right) + \frac{h_\infty}{2} \quad (10)$$

for $0 < |x-r_P| < \lambda_E$ and $z_E(x) = h_\infty/2$ for $|x-r_P| > \lambda_E$ and, similarly,

$$z_I(x) = \frac{\xi_I}{2} \left(\cos \frac{\pi x}{\lambda_I} + 1 \right) - \frac{h_\infty}{2} \quad (11)$$

for $0 < |x| < \lambda_I$ and $z_I(x) = -h_\infty/2$ for $|x| > \lambda_I$; where the membrane response is symmetric with respect to the peptide long axis ($x=0$). Using this profile, the hydrocarbon volume, \mathcal{V} , and the interfacial lipid area, \mathcal{A} , are readily calculated by appropriate integration. For the case $\alpha=\pi$ the embedded peptide volume is $\mathcal{V}_P = \pi r_P^2 l_P/2$. The condition $\mathcal{V} = Nv$ determines the range of integration, which is chosen to be much larger than the lipid perturbation length.

We emphasize that the sinusoidal shape modulation in Eqs. 10 and 11, though approximate, provides a convenient description of the two local monolayer perturbations; characterized by the amplitudes ξ_E and ξ_I and the wavelengths λ_E and λ_I . This is because the combination of ξ_E and ξ_I captures four qualitatively different responses of the membrane, namely: *outward bending* ($\xi_E > 0$ and $\xi_I > 0$), *inward bending* ($\xi_E < 0$ and $\xi_I < 0$), *local compression* ($\xi_E < 0$ and $\xi_I > 0$), and *local stretching* ($\xi_E > 0$ and $\xi_I < 0$). The actual membrane shape is determined by the minimum of the free energy F (see Eq. 4) with respect to ξ_E , ξ_I , λ_E , and λ_I . At this point, we already note that in our numerical calculation (discussed below) we have always found the four unknowns to adjust in such a way that the average cross-sectional area per lipid, \bar{a}_i , remained constant and equal to the corresponding value for an unperturbed, peptide-

free bilayer; $\bar{a}_i = a_0$. This result reflects the fact that changes in interfacial area involve considerably larger energy changes than those associated with chain packing.

Interfacially-adsorbed peptide dimer

The second state we aim to model is that of an interfacially-adsorbed peptide dimer; see Fig. 1b. The geometrical specification we invoke for the dimer is analogous to that of a single peptide. That is, we represent the peptide dimer by two parallel cylinders, each of radius r_P , length l_P , and “hydrophilic” angle α . The two cylinders reside at close contact and both immerse their hydrophobic parts into the bilayer’s chain region. All approximations that we use for the single, isolated, cylinder are used analogously for the dimerized pair of cylinders. In particular, we neglect variations of chain packing characteristics along the y -axis, thus neglecting end effects (which for the dimerized peptide state is a more severe approximation than for an isolated cylinder). Also, we again use Eqs. 10 and 11 (yet, with the replacement $r_P \rightarrow 2r_P$ and a different set of optimized constants ξ_E , ξ_I , λ_E , and λ_I) to describe the membrane shape \mathcal{A} . The interfacial area and the hydrocarbon volume are calculated analogously, as in the case of monomers, only the embedded dimer volume is twice as large, so $\mathcal{V}_P = \pi r_P^2 l_P$.

Pore-forming state

The third state is the pore-forming arrangement shown in Fig. 1c. When assembled into a barrel-stave pore, the peptides are in a transmembrane orientation, forming a ring-like aggregate with their hydrophobic faces in contact with the hydrocarbon core of the host membrane. To calculate the lipid perturbation energy associated with such a pore, we assume that the hydrophobic faces of the transmembrane peptides prescribe a circular wall, impermeable to lipid chains (see Fig. 3). The lipid perturbation free energy in this state is primarily entropic, reflecting the loss of conformational freedom of chains bordering the wall. It should be stressed that our circular wall model for the peptide pore is only appropriate for barrel-stave like pores where, in addition, electrostatic effects are minor. It should also be noted that because the radius of peptide pores is typically considerably larger than the lipid (cross-sectional) dimension, the wall can be safely treated as planar (see the later discussion of the wall approximation). Moreover, the precise topology (and area) of the interface between the peptides and the membrane depends, generally, on the polar angle of the peptide and on the number of peptides, and is frequently affected by the presence of a proline-induced kink in the peptide backbone; as discussed, for example, for melittin by Smith et al. (1994) and for alamethicin by Bak et al. (2001). For the particular case where a proline kink

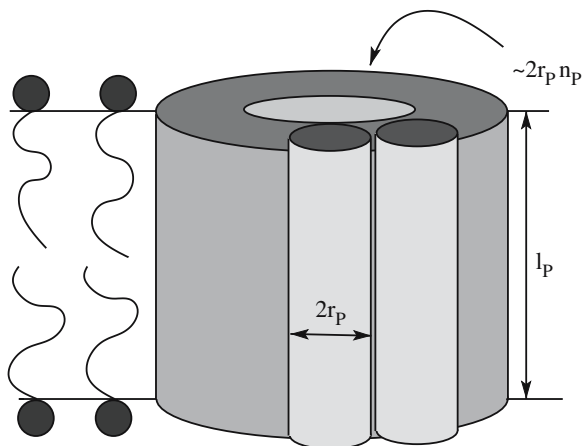


Fig. 3 Schematic illustration of the model for a barrel stave pore. The interfacial area between the peptide-aggregate and the hydrocarbon core is proportional to the number of peptides in the aggregate, n_p , is approximately given by $2 r_p l_p n_p$. The approximation made by replacing the cylinder-like pore geometry by a planar wall is discussed in the section “Discussion of the wall approximation”

exists, the contact area per peptide (and hence its energy) depends on the number of peptides in the aggregate. Interestingly, this finding has been used to explain the dependence of alamethicin pore size distribution on the elastic properties of the lipid host (Cantor 2002; Dan and Safran 1998). The present model neglects the topological details of the aggregate’s interfacial contact and treats it as a smooth wall of height l_p and length $2 r_p$ per peptide (see Fig. 3). The height l_p of the wall generally need not coincide with the thickness h_∞ of the membrane’s hydrocarbon core. The cases $l_p > h_\infty$ and $l_p < h_\infty$ are referred to as positive and negative hydrophobic mismatch, respectively. The presence and degree of hydrophobic mismatch are known to influence the interfacially adsorbed-to-transmembrane transition of peptides in membranes (Ren et al. 1999; Sansom 1993). However, for simplicity, in the present work we model peptides whose length matches the (flat) hydrophobic core thickness, setting $l_p = h_\infty$, and neglecting issues related to hydrophobic mismatch.

Results and discussion

The calculations presented in this section are for lipid bilayers composed of C-12 (Lauric) chains. Our choice of the headgroup repulsion strength, $B = 20k_B T \text{Å}^2$, ensures $a_0 = 29.4 \text{Å}^2$, the equilibrium cross-sectional area per chain in a flat, unperturbed (peptide-free) membrane. This corresponds to a thickness $h_\infty = 2 \nu / a_0 = 22 \text{Å}$ of the unperturbed hydrocarbon core, consistent with experimental studies on dilauroylphosphatidylcholine (DLPC) bilayers (Balgavý et al. 2001). Note that the equilibrium value of a_0 reflects the balance between three competing interactions—attractive at the interfacial region and repulsive within both the headgroup and tail

regions. Consequently, increasing repulsion between headgroups (increasing B) leads to larger values for a_0 .

For a flat bilayer, the magnitude of l does not affect a_0 . However, l affects the propensity of a lipid monolayer to bend, as expressed by the magnitude of the spontaneous curvature c_0 . Qualitatively, larger l shifts c_0 to more positive values. We use $l = 1 \text{Å}$ to represent rather small lipid headgroups (Fattal et al. 1995), and in the section “Influence of spontaneous curvature” discuss the consequences of increasing l .

The peptides modeled in this study have the dimensions: $r_p = 6 \text{Å}$ and $l_p = h_\infty = 22 \text{Å}$. In the present work, we shall focus on one representative case of the peptide polar angle: $\alpha = \pi$, implying a peptide penetration depth of $\approx r_p = 6 \text{Å}$ into the hydrophobic core of the membrane (Hristova et al. 1999). Such peptides have shown to cause the largest lipid chain perturbations (Zemel et al. 2004).

Reference state

We shall use ΔF to denote the free energy of the perturbed membrane, per peptide, relative to the reference state of the flat, unperturbed bilayer (with equilibrium thickness h_∞ everywhere). The corresponding free energy of the reference membrane (for the same number of lipids as in the perturbed system) is denoted by F_0 , so that the membrane perturbation free energy, per peptide, is

$$\Delta F = F - F_0 \quad (12)$$

We emphasize that ΔF stands for the (generally positive) lipid contribution to the binding free energy and lacks the solvation free energy of an isolated peptide which provides the main driving force for its insertion into the membrane. This additional contribution to ΔF is a constant which we set equal to zero. This contribution depends of course on the type of peptide and membrane. Here, however, we consider the membrane-inserted peptide to have the same insertion depth, namely r_p (and hence the same solvation free energy) for all membrane-peptide association states. Direct interactions between peptides are not included in ΔF . The peptide-peptide electrostatic interaction will be evaluated separately and compared with ΔF .

Membrane structure

Figure 4 presents the structural and energetic consequences of the different membrane-peptide association states shown in Fig. 1. Panel (a) shows the energetically optimal membrane structure and the corresponding average conformations of various lipid chains, calculated using the chain packing theory, for two peptides that are inserted individually into the outer monolayer. Each peptide has its hydrophobic part, of angular size $\alpha = \pi$, embedded in the hydrocarbon core. The inter-

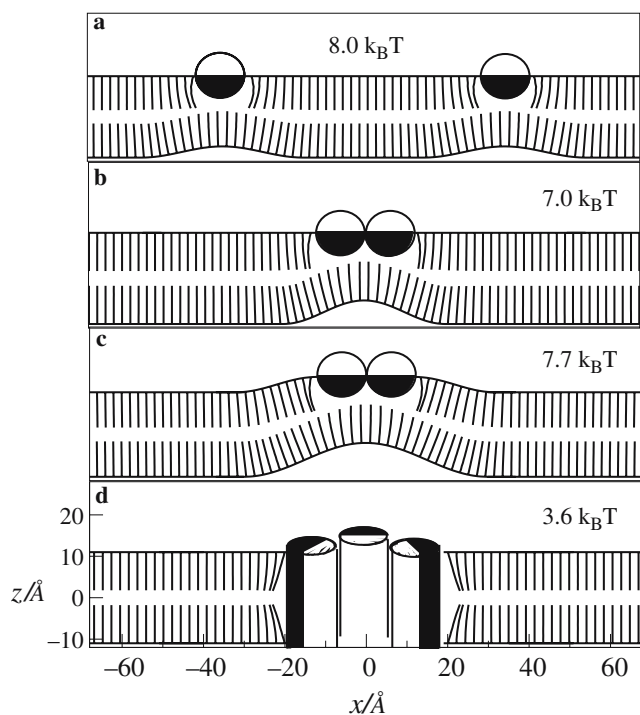


Fig. 4 Cross-sectional membrane structures and the associated perturbation free energies per peptide, ΔF , for various peptide-membrane association states: isolated peptides in the energetically optimal membrane configuration (a), peptide dimer in the energetically optimal state (b), upward bending of the membrane in the dimerized state (c), and the transmembrane pore state of the peptides (d). The interfacially-adsorbed peptides are modeled as rigid cylinders, whereas the pore state is represented by a straight wall. The interfacial surfaces A of the membranes are shown by solid lines. To illustrate the changes in chain packing, we also depict the average conformation of various lipid chains (with the averaged segment positions of the given chain connected by solid lines)

peptide distance is large enough to exclude membrane-mediated peptide-peptide interactions. Panels (b) and (c) of Fig. 4 show a peptide dimer adsorbed at the membrane interface. Panel (b) displays the energetically optimal membrane configuration, and panel (c) shows an alternative, outwardly-bent, membrane configuration. Finally, panel (d) provides the comparison with a membrane pore. The free energies associated with the various configurations are depicted in the figure and discussed in the next section.

The most evident structural consequence of interfacially-bound peptides is a local thinning of the bilayer in the vicinity of the peptides. Thinning of the bilayer, which is much more pronounced in the case of dimers, is intimately related to the creation of a “void” underneath the peptide cylinder, which must be filled by lipid chains. Lipid chains from both monolayers participate in filling these voids—those in the outer monolayer by tilting and splaying, and those in the inner monolayer by stretching (Zemel et al. 2004). One possible way of relieving the stretching deformation stress is to bend the inner monolayer toward the peptide, causing local membrane

thinning. In the case of a dimer, the displacement of lipid chains from the void region is larger and hence it induces a much stronger deformation. A similar conclusion was obtained from an X-ray diffraction study of phosphocholine lipid multilayers, in which the structure of the membrane bound by melittin monomers was compared with that containing its dimeric analogs (Hristova et al. 2001).

Our calculations show that the bending deformation of the inner monolayer toward the outer monolayer is energetically preferable over bending of the outer monolayer toward the inner one (see Fig. 4 panels (a) and (b) and the discussion of Fig. 6 below). Consequently, the membrane thinning deformation is asymmetric. For example, in the case of a monomer, in the membrane’s minimal energy configuration—panel (a)—the inner monolayer is substantially bent toward the peptide ($\xi_I \approx 3$ Å) whereas the outer monolayer maintains its flat state ($\xi_E \approx 0$). In the case of a dimer, this asymmetry is even more pronounced. To explain this observation, we note that monolayer bending generally involves both splay and tilt deformations of the lipid chains in that monolayer (Helfrich 1973). The presence of an adsorbed peptide forces the lipid chains in the outer monolayer to tilt and splay even in a flat monolayer (to fill the “void” underneath the peptide). A bending deformation of the outer monolayer towards the inner one would further increase the splay deformation, with a corresponding quadratic increase in the perturbation free energy (Hamm and Kozlov 2000). Hence, bending of the (previously unsplayed) inner monolayer is energetically less costly than bending of the outer monolayer. Similar considerations apply to the monomeric and dimeric peptide states; the inward bending of the inner monolayer being more pronounced for the dimeric state.

The perturbations induced by either monomeric or dimeric peptides decay within a lateral distance of 20–40 Å; for the monomer, the optimal wavelength of the internal layer is $\lambda_I = 20$ Å (panel a) and for the dimer $\lambda_I = 25$ Å (panel b). Indeed, it is expected that the decay length is comparable to the length of the lipid chains themselves. The lateral structure of a peptide-containing lipid bilayer was recently probed experimentally, using the technique of grazing incidence X-ray diffraction (Münster et al. 2000, 2002). The short-range order of lipid chains in multilamellar bilayers of 1,2-dimyristoyl-sn-glycero-3-phosphatidylcholine (DMPC) was found to be strongly reduced by interfacially-adsorbed magainin 2 molecules, and to decay within 62 Å. The reduced order of chains in the peptide’s vicinity reflects the local thinning of the membrane. The larger decay length obtained in this study could reflect the influence of lipid chain correlations, which are disregarded in our analysis.

Similar conclusions derive from NMR measurements of lipid chain bond orientational order parameters. The orientational order parameter of the C–H bond of carbon atom n along the chain is given by

$$S_n = \frac{1}{2} \langle 3 \cos^2 \theta_n - 1 \rangle \quad (13)$$

where θ_n is the angle between the C_n -H bond and the membrane normal, and the angular brackets indicate averaging over all chain conformations. In a peptide-free membrane, all lipid chains are equivalent, and their order parameter profiles are equal. In the perturbed membrane, the order parameter profiles depend on the chain origin, x . Since the experimentally-measured order parameter profiles involve averaging over all lipid chains, we adopt a similar averaging for calculating the S_n values; that is, the averaging involves all conformations of all lipids in both monolayers. Note that a random distribution of bond orientations leads to $S_n=0$, whereas for a fully stretched (all-trans) chain oriented along the membrane normal $S_n = -1/2$, for all n . Figure 5 compares $-S_n$ for the three cases depicted in panels (a), (b) and (d) of Fig. 4; in other words $-S_n$ for a membrane with adsorbed peptide monomer (bold solid curve), dimer (dashed curve) and a transmembrane peptide (dotted curve), respectively. For comparison, we also plot two additional profiles: one for the unperturbed, peptide-free, flat bilayer (solid curve), and the other for a peptide-free membrane having the same shape deformation as is in the case of the adsorbed monomer (dotted-dashed curve) (see Fig. 4 panel (a)). The lower panel in Fig. 5 displays the peptide-induced change in the C-H bond order parameter, measured relative to the unperturbed membrane,

$$\Delta S_n^{\text{CH}} = S_n - S_n^0 \quad (14)$$

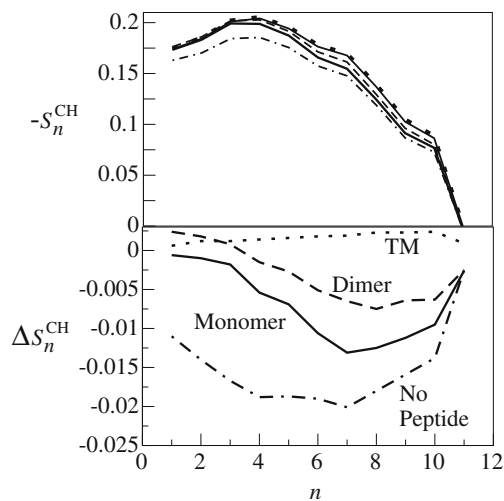


Fig. 5 C-H Bond orientational order parameter profiles (upper panel) and their difference compared with that of the unperturbed membrane (lower panel), for five cases of interest. The *bold solid*, *dashed*, and *dotted* curves are for the monomer, dimer and transmembrane cases shown in Fig. 4, panels (a), (b) and (d), respectively. These curves are compared in the text with those of the unperturbed, peptide-free, flat membrane (*solid* curve); and with that of a peptide-free bilayer deformed in the same way as shown in panel (a) of Fig. 4 for the monomer (*dotted-dashed*)

where S_n^0 is the C_n -H bond order parameter profile of the peptide-free membrane.

The results we find for the unperturbed bilayer are in good agreement with NMR measurements of DLPC membranes (Douliez et al. 1995).

Qualitatively, local thinning leads to reduced chain order. To distinguish this effect from the more complex effect resulting from peptide adsorption we plot the profile obtained for a peptide-free membrane undergoing local thinning (dotted-dashed curve). Characteristically, all lipid segments become less ordered, but those in the middle are more affected. Compared to the latter effect, a monomer, and even more pronounced, a dimer, increases the order of chain segments. This effect is due to stretching of chains, mainly from the internal layer, to reach the region underneath the peptide. Nevertheless, when compared to the unperturbed membrane, the chains are more disordered. Qualitatively, the same behavior—including a peptide-induced thinning of the chain region of roughly 2Å—has been observed experimentally by Koenig et al. (1999), based on deuterium order parameter profiles for membrane-bound amphipathic peptide fragments of the envelope protein of human immunodeficiency virus Type I (HIV-1). Comparable results have also been obtained in a recent molecular-dynamics simulation of two antimicrobial peptides in the presence of a lipid bilayer (Shepherd et al. 2003). Membrane thickness and chain order parameters are seen to decrease as the peptide penetrates into the membrane. The order parameter profiles plotted for the last 10 ns (where the peptide already penetrates the hydrophobic core of the membrane) are in good qualitative and quantitative agreement with our chain packing calculations.

In marked contrast to the effect of adsorbed peptides, transmembrane peptides do not induce any significant change in S_n (as long as no hydrophobic mismatch exists). In fact, a careful inspection of Fig. 5 (lower panel) reveals a slight ordering of the chains. This is a typical consequence of the “ordering effect” of the peptide wall (Fattal and Ben-Shaul 1993).

A more detailed structural and energetical analysis is presented in Fig. 6, summarizing all calculations performed with optimized choices of the parameters λ_E and λ_I , for both the monomeric and dimeric states. Each contour marks changes of $0.4 k_B T$ per inclusion (monomer or dimer), demonstrating the free energy scale within which shape modulations occur. For clarity, the ξ_E, ξ_I plane is divided into sections, accounting for the qualitatively different shape modulations as outlined in the “Theory” section. Generally, we observe two possible types of membrane modulations. The global free energy minimum is adopted at vanishing perturbation amplitude of the outer layer ($\xi_E = 0$) and for positive value of the inner layer ($\xi_I > 0$), ranging between 1 and 5 Å in the case of a monomer and between 4 and 10 Å for the dimer. The type of modulation that is close in free energy to the global minimum can either be classified as local “compression”, where the inner layer is locally

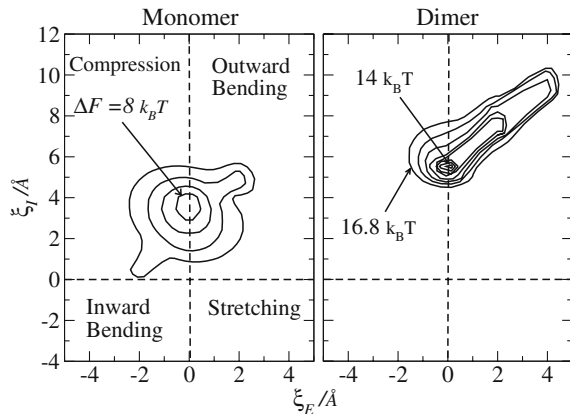


Fig. 6 Free energy contour plots in the ζ_E , ζ_I plane, shown separately for an interfacially-adsorbed monomer and dimer. Each contour (starting from the middle) corresponds to a $0.4 k_B T$ increase in the perturbation free energy, measured per monomer and per dimer, respectively, relative to the unperturbed membrane. The ζ_E , ζ_I plane is divided into four regions, with the corresponding deformation modes indicated. Note the asymmetry in the response of the two membrane layers

pushed toward the peptide whereas the outer layer bends in the opposite direction ($\zeta_I > 0$ and $\zeta_E < 0$), or as local “outward bending” where both layers shift outwardly in the same direction. In most cases, especially for the dimer, this modulation mode involves local compression (or thinning) of the bilayer; $\zeta_I > \zeta_E$. Illustrations of the two most favorable modulation modes are depicted for the dimeric case in panels (b) and (c) of Fig. 4. Comparing the steepness of the two contour plots, we find that the dimer, to a greater extent than the monomer, rigidifies the membrane with respect to shape modulations.

To the best of our knowledge, no experimental or theoretical evidence exists which describes the asymmetric response of the bilayer. However, asymmetry is expected for a non-symmetric distribution of peptides within the two layers. The structural consequences listed above should hold as long as the peptides penetrate only a little into the membrane. For deeper penetrations the asymmetric response is likely to be different. This point is under current investigation.

Free energies of peptide–membrane complexes

We now discuss the free energies of the three membrane states depicted schematically in Fig. 1, whose detailed calculation is displayed in Fig. 4. At the energetically optimal membrane configuration, the lipid perturbation free energy associated with adsorbing a monomeric peptide at the membrane interface is $\Delta F = 8.0 k_B T$, panel (a). The corresponding free energy of a dimeric peptide is shown in panels (b) and (c). In the minimal free energy configuration—panel (b)—the perturbation free energy is $\Delta F = 7.0 k_B T$ per peptide, somewhat lower than for the monomeric state. This indicates a small but notable free

energy gain due to the lipid membrane, favoring (energetically) peptide dimerization. Panel (c) also displays the dimeric peptide state, but for a somewhat outwardly-bent membrane configuration; the corresponding perturbation free energy per peptide, $\Delta F = 7.7 k_B T$, is only marginally larger than the optimal one, suggesting large thermal fluctuations of the peptide–membrane complex. Finally, for the transmembrane, pore-forming, peptide orientation—panel (d)—the corresponding membrane perturbation free energy per peptide is $\Delta F = 3.6 k_B T$, substantially lower than for any of the interfacially-adsorbed peptide states (monomeric or dimeric).

From Fig. 4, the surrounding lipid medium provides a strong driving force toward helix reorientation (insertion) and a weaker tendency for interfacially-adsorbed peptides to self-assemble. The free energy gain upon peptide reorientation is about $4 k_B T$ per peptide but only $1 k_B T$ for interfacial dimerization. Because amphipathic peptides are typically charged, we expect an additional repulsive interaction to oppose the peptides’ tendency to self-assemble. This additional repulsion will depend on the overall net charge of the peptides.

Consider first the dimerization, shown in panels (a) and (b) of Fig. 4. Using Poisson-Boltzmann theory, we calculated the change in electrostatic energy, ΔF_{el} , upon dimerization of two peptide-cylinders for two representative cases: weakly-charged peptides, with net charge 1 (for example alamethicin), and highly-charged peptides, with net charge 4 (for instance magainin). We ignore the possible role of lipid headgroup charges (such as partial screening effects that arise from oppositely-charged lipid headgroups) and assume a physiological salt concentration of 0.1 M. Treating the overall charge as uniformly distributed over the hydrophilic face of the peptide, we obtain $\Delta F_{el} = 0.2 k_B T$ and $\Delta F_{el} = 1.7 k_B T$ for the weakly and highly-charged peptides, respectively. (For a detailed account of a similar electrostatic calculation, see Zemel et al. (2003)). We thus conclude that weakly-charged adsorbed peptides are likely to experience a net attraction, whereas highly-charged peptides repel each other. It should also be remembered that peptide association is unfavorable on entropic grounds. These differences could be relevant for pore formation, namely if interfacial self-association occurs as an intermediate step, as experiments indeed suggest (Takei et al. 1999; Dempsey et al. 2003; Hristova et al. 2001).

In most cases, pore formation requires the aggregation of more than two amphipathic peptides; dimerization is only the first essential step. However, the role of the membrane in the process follows from a generic tendency of the lipid chains to minimize their contact area with the surface of the peptides. Consider, for example, the dimeric state shown in Fig. 4b; introducing a third (previously monomeric) peptide in-between the two peptides results in the liberation of two of its contact surfaces with the membrane, and thus lowers ΔF . A similar tendency would drive the insertion of an additional peptide into a pre-existing transmembrane (and pore-forming) aggregate—at even larger gain of free

energy. The following questions then arise: how many peptides are required, and along which path does the orientational change from a membrane-inserted to a transmembrane state proceed? Clearly answers to these questions are not currently available.

Electrostatic interactions play a major role in determining the structure and energetics of transmembrane pores, especially the relative stability of barrel-stave versus toroidal pores. Based on Poisson-Boltzmann theory, it was argued that only weakly-charged peptides should assemble into barrel-stave pores, whereas highly-charged peptides are predicted to form toroidal pores (to which our wall-like pore model is not applicable) (Zemel et al. 2003). The electrostatic free energy associated with reorientation of a singly charged peptide into a barrel-stave pore is $\Delta F_{el} \approx 1.5k_B T$, considerably weaker than the lipid perturbation driving force $\Delta F \approx -4k_B T$.

We thus conclude that, at least for weakly-charged peptides, electrostatic interactions are likely to be negligible in comparison to the structural membrane (lipid chain) perturbation effects. The latter provide the main driving force for the cooperative transition of several interfacially-adsorbed (and possibly pre-aggregated) peptides into a transmembrane pore. This is the central conclusion of the present work.

Influence of spontaneous curvature

Finally, we consider the role of l (Fig. 2), the distance between the hydrocarbon-water interface and the plane within which headgroup repulsion is most pronounced. This parameter, along with the headgroup repulsion strength B , is directly related to the spontaneous curvature of the lipids (May and Ben-Shaul 1999, May 2000). With larger values of l , corresponding to a larger positive spontaneous curvature, the membrane turns more resistive to acquire the negative curvature needed in the internal layer; the “outward bending” mode is restricted and the perturbation free energy increases. Hence, increasing the proportion of lipids with negative spontaneous curvature in a lipid mixture is expected to stabilize the adsorbed state, and might hinder pore formation, as was suggested experimentally (Heller et al. 1997; Matsuzaki et al. 1995).

A simple model for the energetics of pore formation

The energetics of pore formation can be rationalized in terms of a simple analytical “director” model, which has recently been shown to be in good qualitative agreement with detailed chain packing calculations (May and Ben-Shaul 2000). In this model, the hydrocarbon chain is represented by a rigid fluctuating vector, oriented along the main chain axis (which, for convenience, may be identified with the end-to-end vector). The “director,” which originates at the lipid headgroup, is allowed to adopt all orientations within the hydrocarbon core with

equal probability; however, it cannot penetrate through walls, like the surface of an amphipathic peptide which can roughly be modeled as a monolayer-spanning rigid wall. Assuming statistical independence of all directors, the presence of a wall results in orientational (chain conformational) free energy penalty of

$$\Delta F = (1 - \ln 2)k_B T \frac{h_\infty}{2a_0} \quad (15)$$

per monolayer (May and Ben-Shaul 2000). Here, L is the length of the wall, h_∞ (in our system 22 Å) is the thickness of the hydrophobic bilayer region, and a_0 ($\approx 30 \text{ \AA}^2$) is the cross-sectional area per hydrocarbon chain.

First consider the pore state shown in Fig. 4d. Using Eq. 15 for a single bilayer-spanning wall of length $L = 2 \times 2 \times r_P$ (the additional factor of 2 accounts for the two monolayers that contribute to a bilayer) we find a perturbation free energy of $\Delta F = 2.7k_B T$. The difference from the value $3.6 k_B T$ found using the chain packing theory (Fig. 4d) can be explained by additional elastic interactions that are not accounted for by the director model (May 2002). Consider now the interfacially-adsorbed monomeric state shown in Fig. 4a. The appropriate wall length (accounting for the two membrane-interacting faces of the peptide) is $L = 2l_P = 44 \text{ \AA}$, for which we obtain $\Delta F = 5.0 k_B T$. The difference from the value, $\Delta F = 8.0 k_B T$, found by the chain-packing calculations (see panel (a) of Fig. 4), can again be explained by additional elastic deformations of the two lipid monolayers, particularly the inner one which is subject to a considerable bending deformation.

The director model predicts a free energy gain of $\Delta F = 2.5k_B T$ per peptide for the aggregation of two peptides. However, at the same time the elastic deformation of the inner monolayer is also increased, which partially compensates the gain in free energy and explains the relatively small value ($\Delta F = 1.0k_B T$) found using the chain-packing calculations (see panel (b) of Fig. 4).

Discussion of the wall approximation

In this work, we have approximated the (geometrically rather complex) transmembrane pore state using simply a straight wall. The energetic penalty for the lipids in the vicinity of the wall results mainly from restrictions in conformational freedom of the hydrocarbon chains. One may argue that a cylinder-like inclusion (instead of a flat wall), with the cylinder radius $R \approx 20 \text{ \AA}$ corresponding to that of a barrel-stave pore, would be a more appropriate model for calculating ΔF . Indeed, using a *curved* wall (with radius of curvature $1/R$) will affect ΔF . Again, the director model provides a convenient tool to estimate the corresponding difference; a chain-packing calculation is expected to make similar predictions. Based on the director model, the calculation (see Fig. 8 of Kessel et al. 2001) results in a *decrease* of ΔF for a cylinder of

radius $R \approx 20 \text{ \AA}$ and a director length of $h_\infty/2 = 11 \text{ \AA}$ of about 20 %. (Application to Fig. 4d results in $2.9k_B T$ instead of $3.6k_B T$.) This decrease is a result of the additional gain in conformational freedom if a lipid faces a cylinder-like wall instead of a flat wall. Yet, the magnitude of this decrease is certainly negligibly small compared to the large energetic differences found in Fig. 4 for pore formation.

Concluding remarks

In this work, we have studied the perturbation of lipid organization upon the adsorption of amphipathic peptides onto a membrane surface and the subsequent formation of a peptide-decorated aqueous pore. We have analyzed in considerable detail the possible dimerization of interfacially-adsorbed peptides within the membrane plane, since dimers are believed to serve as precursors in the formation of membrane pores. Our calculations suggest that dimerization of two well-separated peptides indeed results in lower lipid perturbation free energy, reflecting the smaller “contact area” between the peptides’ surface and the surrounding lipids. For strongly-charged peptides, this tendency for peptide association may be counterbalanced by strong electrostatic repulsions. Weakly-charged peptides, on the other hand, may indeed associate at the membrane plane and eventually undergo a cooperative orientational transition to form a barrel-stave pore. Our calculations suggest that this latter transition is strongly favored by the lower lipid perturbation free energy in the pore state. It must be remembered however that the orientational transition from the adsorbed (“horizontal”) to inserted (pore, “vertical”) state may involve a substantial activation-free energy barrier, which we have not attempted to calculate here.

Acknowledgments A.Z. thanks the Yeshaya Horowitz Foundation for a doctoral fellowship. S.M. thanks the Thüringer Ministerium für Wissenschaft, Forschung und Kunst. The financial support of the Israel Science Foundation (grant 227/02) and the United States-Israel Binational Science Foundation (grant 2002-75) is gratefully acknowledged. The Fritz Haber Center is supported by the Minerva Foundation, Munich, Germany.

References

- Bak M, Bywater RP, Hohwy M, Thomsen JK, Adelhorst K, Jakobsen H, Sorensen OW, Nielsen NC (2001) Conformation of alamethicin in oriented phospholipid bilayers determined by $(15)\text{N}$ solid-state nuclear magnetic resonance. *Biophys J* 81:1684–1698
- Balgavý P, Dubničková M, Kučerka N, Kieslev MA, Yaradaikin S, Uhriková D (2001) Bilayer thickness and lipid interface area in unilamellar extruded 1,2-diacylphosphatidylcholine liposomes: a small-angle neutron scattering study. *Biochim Biophys Acta* 1512:40–52
- Bechinger B (1999) The structure, dynamics and orientation of antimicrobial peptides in membranes by multidimensional solid-state NMR spectroscopy. *Biochim Biophys Acta* 1462:157–183
- Ben-Shaul A, Gelbart WM (1994) Statistical thermodynamics of amphiphile self-assembly: structure and phase transitions in micellar solutions. In: Gelbart WM, Ben-Shaul A, Roux D (eds) *Micelles, membranes, microemulsions and monolayers*. Springer, New York, Ch1, pp 359–402
- Cantor RS (2002) Size distribution of barrel-stave aggregates of membrane peptides: Influence of the bilayer lateral pressure profile. *Biophys J* 82:2520–2525
- Chen L, Bassolino D, Stouch T (1997) Transmembrane helix structure, dynamics, and interactions: Multi-nanosecond molecular dynamics simulation. *Biophys J* 73:3–20
- Dan N, Safran SA (1998) Effect of lipid characteristics on the structure of transmembrane proteins. *Biophys J* 75:1410–1414
- Dempsey CE, Ueno S, Avison MB (2003) Enhanced membrane permeabilization and antibacterial activity of a disulfide-dimerized magainin analogue. *Biochemistry* 42:402–409
- Douliez JP, Léonard A, Dufourc EJ (1995) Restatement of order parameters in biomembranes: calculation of C-C bond order parameters from C-D quadrupolar splittings. *Biophys J* 68:1727–1739
- Fattal DR, Ben-Shaul A (1993) A molecular model for lipid protein interaction in membranes: the role of hydrophobic mismatch. *Biophys J* 65:1795–1809
- Fattal DR, Andelman D, Ben-Shaul A (1995) The vesicle-micelle transition in mixed lipid-surfactant systems: a molecular model. *Langmuir* 11:1154–1161
- Hamm M, Kozlov MM (2000) Elastic energy of tilt and bending of fluid membranes. *Eur Phys J B* 3:323–335
- He K, Ludtke SJ, Heller WT, Huang HW (1996) Mechanism of alamethicin insertion into lipid bilayers. *Biophys J* 71:2669–2679
- Helfrich W (1973) Elastic properties of lipid bilayers: theory and possible experiments. *Z Naturforsch* 28:693–703
- Heller WT, He K, Ludtke SJ, Harroun TA, Huang HW (1997) Effect of changing the size of lipid headgroup on peptide insertion into membranes. *Biophys J* 73:239–244
- Hristova K, Wimley WC, Mishra VK, Anantharamiah GM, Segrest JP, White SH (1999) An amphipathic α -helix at the membrane interface: A structural study using a novel X-ray diffraction method. *J Mol Biol* 290:99–117
- Hristova K, Dempsey CE, White SH (2001) Structure, location, and lipid perturbations of melittin at the membrane interface. *Biophys J* 80:801–811
- Huang HW, Wu Y (1991) Lipid-alamethicin interactions influence alamethicin orientation. *Biophys J* 60:1079–1087
- Huang HW, Chen FY, Lee MT (2004) Molecular mechanism of peptide-induced pores in membranes. *Phys Rev Lett* 92:198304
- Israelachvili JN (1992) *Intermolecular and surface forces*, 2nd edn. Academic, New York
- Kessel A, Ben-Tal N, May S (2001) Interactions of cholesterol with lipid bilayers: The preferred configuration and fluctuations. *Biophys J* 81:643–658
- Koenig BW, Ferretti JA, Gawrisch K (1999) Site-specific deuterium order parameters and membrane-bound behavior of a peptide fragment from the intracellular domain of HIV-1 gp41. *Biochemistry* 38:6327–6334
- Lin J, Baumgaertner A (2000) Stability of a melittin pore in a lipid bilayer: a molecular dynamics study. *Biophys J* 78:1714–1724
- Ludtke SJ, He K, Wu Y, Huang HW (1994) Cooperative membrane insertion of magainin correlated with its cytolytic activity. *Biochim Biophys Acta* 1190:181–184
- Ludtke SJ, He K, Huang HW (1995) Membrane thinning caused by magainin 2. *Biochemistry* 34:16764–16769
- Ludtke SJ, He K, Heller WT, Harroun TA, Yang L, Huang HW (1996) Membrane pores induced by magainin. *Biochemistry* 35:13723–13728
- Matsuzaki K, Sugishita K, Fujii N, Miyajima K (1995) Molecular basis of membrane selectivity of an antimicrobial peptide, magainin 2. *Biochemistry* 34:3423–3429
- Matsuzaki K, Sugishita K, Ishibe N, Ueha M, Nakata S, Miyajima K, Epand RM (1998) Relationship of membrane curvature to the formation of pores by magainin 2. *Biochemistry* 37:11856–11863

- May S (2000) Protein-induced bilayer deformations: The lipid tilt degree of freedom. *Eur Biophys J* 29:17–28
- May S (2002) Membrane perturbations induced by integral proteins: role of conformational restrictions of the lipid chains. *Langmuir* 18:6356–6364
- May S, Ben-Shaul A (1999) Molecular theory of lipid-protein interaction and the L_{α} - L_{II} transition. *Biophys J* 76:751–767
- May S, Ben-Shaul A (2000) A molecular model for lipid-mediated interaction between proteins in membranes. *Phys Chem Chem Phys* 2:4494–4502
- Münster C, Lu J, Schinzel S, Bechinger B, Salditt T (2000) Grazing incidence x-ray diffraction of highly aligned phospholipid membranes containing the antimicrobial peptide magainin 2. *Eur Biophys J Biophys Lett* 28:683–688
- Münster C, Spaar A, Bechinger B, Salditt T (2002) Magainin 2 in phospholipid bilayers: peptide orientation and lipid chain ordering studied by x-ray diffraction. *Biochim biophys Acta* 1562:37–44
- Oren Z, Shai Y (1998) Mode of action of linear amphipathic alpha-helical antimicrobial peptides. *Biopolymers* 47:451–463
- Rapaport D, Shai Y (1991) Interaction of fluorescently labeled pardaxin and its analogues with lipid bilayers. *J Biol Chem* 266:23769–23775
- Rapaport D, Shai Y (1992) Aggregation and organization of pardaxin in phospholipid membranes. A fluorescence energy transfer study. *J Biol Chem* 267:6502–6509
- Rapaport D, Peled R, Nir S, Shai Y (1996) Reversible surface aggregation in pore formation by paradaxin. *Biophys J* 70:2502–2512
- Ren J, Lew S, Wang Z, London E (1999) Control of the transmembrane orientation and interhelical interactions within membranes by hydrophobic helix length. *Biochemistry* 38:5905–5912
- Sansom MSP (1993) Alamethicin and related peptaibols-model ion channels. *Eur Biophys J* 22:105–124
- Schwarz G, Stankowski S, Rizzo V (1986) Thermodynamic analysis of incorporation and aggregation in a membrane: application to the pore-forming peptide alamethicin. *Biochim Biophys Acta* 861:141–151
- Shepherd CM, Vogel HJ, Tieleman DP (2003) Interactions of the designed antimicrobial peptide MB21 and truncated dermaseptin S3 with lipid bilayers: molecular-dynamics simulations. *Biochem J* 370:233–243
- Smith R, Separovic F, Milne TJ, Whittaker A, Bennett FM, Cornell BA, Makriyannis A (1994) Structure and orientation of the pore-forming peptide, melittin, in lipid bilayers. *J Mol Biol* 241:456–466
- Takei J, Remenyi A, Dempsey CE (1999) Generalized bilayer perturbation from peptide helix dimerization at membrane surfaces: vesicle lysis induced by disulphide-dimerised melittin analogues. *FEBS Lett* 442:11–14
- Yang L, Weiss TM, Lehrer RI, Huang HW (2000) Crystallization of antimicrobial pores in membranes: magainin and protegrin. *Biophys J* 79:2002–2009
- Yang L, Harroun TA, Weiss TM, Ding L, Huang HW (2001) Barrel-Stave model or Toroidal model? A case study on melittin pores. *Biophys J* 81:1475–1485
- Zemel A, Fattal DR, Ben-Shaul A (2003) Energetics and self-assembly of amphipathic peptide pores in lipid membranes. *Biophys J* 84:2242–2255
- Zemel A, Ben-Shaul A, May S (2004) Membrane perturbation induced by interfacially adsorbed peptides. *Biophys J* 86:3607–3619
- Zuckermann MJ, Heimburg T (2001) Insertion and pore formation driven by adsorption of proteins onto lipid bilayer membrane-water interfaces. *Biophys J* 81:2458–2472